Supplemental Material: Steady Rayleigh–Bénard convection between no-slip boundaries

Baole Wen[1]†, David Goluskin[2]‡, and Charles R. Doering[1,3,4]

[1]Department of Mathematics, University of Michigan, Ann Arbor, MI 48109-1043, USA

[2]Department of Mathematics & Statistics, University of Victoria, Victoria, BC, V8P 5C2, Canada

[3]Department of Physics, University of Michigan, Ann Arbor, MI 48109-1040, USA

[4]Center for the Study of Complex Systems, University of Michigan, Ann Arbor, MI 48109-1042, USA

1. Numerical solutions

Tables 1S to 3S give the Nu, k, and Re values for numerical solutions with $Pr = 1$ and $\Gamma = 2$, Γ^*, and Γ^*_{loc}, respectively.

Table 1S: Details for numerical solutions with $Pr = 1$ and $\Gamma = 2$, including the resolution of Fourier modes (N_x) and Chebyshev collocation points (N_z).

Ra	Pr	$k = 2\pi/\Gamma$	$N_x \times N_z$	Nu	Re
$10^{13/4}$	1	π	128×65	1.056590	1.617336
1.9×10^3	1	π	128×65	1.145807	2.682155
2×10^3	1	π	128×65	1.212037	3.317190
2.25×10^3	1	π	128×65	1.355410	4.550975
2.5×10^3	1	π	128×65	1.474455	5.537770
2.75×10^3	1	π	128×65	1.575599	6.391812
3×10^3	1	π	128×65	1.663162	7.159844
$10^{14/4}$	1	π	128×65	1.714193	7.624400
3.5×10^3	1	π	128×65	1.808754	8.526064
4×10^3	1	π	128×65	1.926775	9.740578
4.5×10^3	1	π	128×65	2.025985	10.85141
5×10^3	1	π	128×65	2.111714	11.88534
$10^{15/4}$	1	π	128×65	2.204811	13.09152
8×10^3	1	π	128×65	2.476330	17.05494
10^4	1	π	128×65	2.648664	20.07400
$10^{17/4}$	1	π	128×65	3.122843	29.50047
$10^{18/4}$	1	π	128×65	3.665041	42.29585
$10^{19/4}$	1	π	128×65	4.287042	59.56858
10^5	1	π	128×65	4.994322	82.84462
$10^{21/4}$	1	π	128×65	5.795869	114.2355
$10^{22/4}$	1	π	128×97	6.703915	156.5252

† Email address for correspondence: baolew@umich.edu
‡ Email address for correspondence: goluskin@uvic.ca

$10^{23/4}$	1	π	128×97	7.732236	213.4031
10^{6}	1	π	128×97	8.896615	289.7982
$10^{25/4}$	1	π	256×97	10.21546	392.2837
$10^{26/4}$	1	π	256×129	11.71065	529.6372
$10^{27/4}$	1	π	256×129	13.40898	713.6005
10^{7}	1	π	512×129	15.34493	959.9367
1.35×10^{7}	1	π	512×129	16.46456	1119.932
1.5×10^{7}	1	π	512×129	16.87881	1182.172
1.6×10^{7}	1	π	512×193	17.13944	1222.005
1.65×10^{7}	1	π	512×193	17.26636	1241.484
1.7×10^{7}	1	π	512×193	17.39216	1260.709
1.736×10^{7}	1	π	512×193	17.48282	1274.414
1.76×10^{7}	1	π	512×193	17.54351	1283.493
$10^{29/4}$	1	π	512×193	17.58987	1290.377
1.786×10^{7}	1	π	512×193	17.60946	1293.277
1.8×10^{7}	1	π	512×193	17.64500	1298.522
1.85×10^{7}	1	π	512×193	17.77160	1317.122
1.9×10^{7}	1	π	512×193	17.89693	1335.501
1.95×10^{7}	1	π	512×193	18.02044	1353.657
2×10^{7}	1	π	512×193	18.14193	1371.593
2.4×10^{7}	1	π	512×193	19.04221	1507.890
2.8×10^{7}	1	π	512×193	19.83413	1633.418
$10^{30/4}$	1	π	512×193	20.47798	1739.647
4.5×10^{7}	1	π	512×193	22.44036	2087.182
$10^{31/4}$	1	π	512×193	23.76002	2340.822
10^{8}	1	π	768×257	27.50669	3144.931
$10^{33/4}$	1	π	768×257	31.81154	4220.616
2.15×10^{8}	1	π	768×257	33.36657	4649.541
$10^{34/4}$	1	π	768×257	36.75427	5658.648
4.64×10^{8}	1	π	896×321	40.44652	6875.704
$10^{35/4}$	1	π	896×321	42.42917	7580.057
10^{9}	1	π	1024×321	48.94284	10145.79
$10^{37/4}$	1	π	1024×321	56.42926	13571.10
2.15×10^{9}	1	π	1024×321	59.13988	14935.81
2.5×10^{9}	1	π	1024×321	61.38714	16116.94
$10^{38/4}$	1	π	1024×321	65.06338	18145.61
$10^{153/16}$	1	π	1024×321	67.42466	19511.79
4×10^{9}	1	π	1024×321	68.96487	20429.24
4.64×10^{9}	1	π	1024×321	71.58241	22019.93
$10^{39/4}$	1	π	1024×321	75.09725	24262.22
10^{10}	1	π	1024×321	86.68318	32430.06
$10^{41/4}$	1	π	1024×321	100.0909	43339.02
2×10^{10}	1	π	1024×321	103.0738	45995.60
2.15×10^{10}	1	π	1024×321	104.9517	47705.08

Table 2S: Details for numerical solutions with $Pr = 1$ and the aspect ratios Γ^* that globally maximize $Nu(\Gamma)$, including the resolution of Fourier modes (N_x) and Chebyshev collocation points (N_z).

Ra	Pr	$k = 2\pi/\Gamma^*$	$N_x \times N_z$	Nu	Re
$10^{13/4}$	1	3.116683	128 × 65	1.056697	1.619793
1.9×10^3	1	3.123537	128 × 65	1.145870	2.683859
2×10^3	1	3.128360	128 × 65	1.212070	3.318462
2.25×10^3	1	3.143491	128 × 65	1.355411	4.550777
2.5×10^3	1	3.161280	128 × 65	1.474516	5.535574
2.75×10^3	1	3.180831	128 × 65	1.575828	6.387203
3×10^3	1	3.202416	128 × 65	1.663668	7.152347
$10^{14/4}$	1	3.216383	128 × 65	1.714937	7.614958
3.5×10^3	1	3.247094	128 × 65	1.810118	8.512058
4×10^3	1	3.292192	128 × 65	1.929322	9.719380
4.5×10^3	1	3.329096	128 × 65	2.029942	10.82473
5×10^3	1	3.378413	128 × 65	2.117243	11.84892
$10^{15/4}$	1	3.426419	128 × 65	2.212421	13.04623
8×10^3	1	3.575467	128 × 65	2.492199	17.05494
10^4	1	3.665236	128 × 65	2.671348	19.99537
$10^{17/4}$	1	3.880392	128 × 65	3.171063	29.49222
$10^{18/4}$	1	4.118841	128 × 65	3.757873	42.57254
$10^{19/4}$	1	4.419469	128 × 89	4.454688	60.44520
10^5	1	4.793529	128 × 89	5.278963	84.69567
$10^{21/4}$	1	5.242992	128 × 129	6.252782	117.4323
$10^{22/4}$	1	5.782949	128 × 129	7.404680	161.3367
$10^{23/4}$	1	6.420133	128 × 129	8.769978	219.8304
10^6	1	7.171170	128 × 129	10.39171	297.1691
$10^{25/4}$	1	8.051634	128 × 129	12.32188	398.7272
$10^{26/4}$	1	9.073939	128 × 129	14.62274	531.4357
5×10^6	1	9.997275	192 × 257	16.76769	665.2339
$10^{27/4}$	1	10.25059	192 × 257	17.36827	704.3108
10^7	1	11.59439	192 × 257	20.64616	929.1624
$10^{29/4}$	1	13.12083	192 × 257	24.56044	1221.405
3×10^7	1	14.68186	256 × 257	28.77198	1562.064
$10^{30/4}$	1	14.84741	256 × 257	29.23512	1601.174
$10^{31/4}$	1	16.80072	256 × 257	34.81847	2094.287
10^8	1	18.99815	256 × 321	41.48855	2735.227
$10^{33/4}$	1	21.45545	256 × 321	49.46027	3569.756
3×10^8	1	23.89666	256 × 321	58.05030	4550.127
$10^{34/4}$	1	24.15059	256 × 321	58.99612	4663.393
$10^{35/4}$	1	26.84021	256 × 321	70.43089	6139.224
6×10^8	1	27.08270	256 × 321	71.85714	6344.418
6.5×10^8	1	27.31152	256 × 321	73.66207	6619.142
7×10^8	1	27.35757	256 × 321	75.37932	6911.933
7.5×10^8	1	26.83143	256 × 321	77.02411	7294.891
8×10^8	1	26.28179	256 × 321	78.61210	7683.031
8.5×10^8	1	26.25586	256 × 321	80.14209	7971.925
9×10^8	1	26.36825	256 × 321	81.61573	8227.378

9.5×10^8	1	26.54403	256 × 321	83.03697	8462.830
10^9	1	26.73696	256 × 321	84.40976	8687.394
$10^{37/4}$	1	29.78702	512 × 449	101.5246	11462.12
$10^{38/4}$	1	33.65968	512 × 449	122.1559	14978.49
$10^{39/4}$	1	38.04901	512 × 449	146.9986	19554.08
10^{10}	1	42.83017	512 × 449	176.9293	25585.09
$10^{41/4}$	1	48.06231	512 × 449	213.0247	33536.66
$10^{42/4}$	1	53.90331	512 × 449	256.5802	43967.29
$10^{43/4}$	1	60.50367	512 × 513	309.1454	57597.49
10^{11}	1	67.95755	512 × 513	372.5844	75402.24
$10^{45/4}$	1	76.33729	512 × 769	449.1508	98685.64
$10^{46/4}$	1	85.71701	512 × 897	541.5753	129175.9
$10^{47/4}$	1	96.12138	512 × 897	653.1727	169237.3
10^{12}	1	107.6085	512 × 897	787.9764	221995.2
$10^{49/4}$	1	120.1234	512 × 897	950.9070	291852.5
$10^{50/4}$	1	133.7508	512 × 897	1147.971	384498.9
$10^{51/4}$	1	148.8836	512 × 1025	1386.450	506738.9
10^{13}	1	166.3042	512 × 1025	1675.036	666086.2
$10^{53/4}$	1	186.3974	512 × 1025	2024.094	873176.4
$10^{54/4}$	1	209.4395	512 × 1281	2446.172	1142290
$10^{55/4}$	1	235.2120	512 × 1537	2956.470	1494811
10^{14}	1	263.0987	512 × 1793	3573.640	1962459

Table 3S: Details for numerical solutions with $Pr = 1$ and the aspect ratios Γ^*_{loc} that locally maximize $Nu(\Gamma)$, including the resolution of Fourier modes (N_x) and Chebyshev collocation points (N_z).

Ra	Pr	$k = 2\pi/\Gamma^*_{loc}$	$N_x \times N_z$	Nu	Re
$10^{22/4}$	1	14.09456	96 × 129	5.864201	82.92705
$10^{23/4}$	1	16.41959	96 × 129	6.914669	105.6969
10^6	1	18.89401	96 × 129	8.148261	135.6083
$10^{25/4}$	1	21.66773	96 × 129	9.587445	173.8004
$10^{26/4}$	1	24.88046	96 × 129	11.26803	221.7384
5×10^6	1	27.86575	96 × 129	12.81012	267.8677
$10^{27/4}$	1	28.70377	96 × 129	13.23878	280.9653
10^7	1	33.19466	96 × 129	15.56038	354.6158
$10^{29/4}$	1	38.29704	96 × 129	18.29931	448.0501
3×10^7	1	43.50700	96 × 193	21.21050	554.8653
$10^{30/4}$	1	44.06680	96 × 193	21.52859	566.9565
$10^{31/4}$	1	50.67686	96 × 193	25.33533	717.1889
10^8	1	58.31124	96 × 193	29.82540	906.1212
$10^{33/4}$	1	67.11615	128 × 321	35.12519	1143.903
3×10^8	1	76.25123	128 × 321	40.76618	1413.329
$10^{34/4}$	1	77.23740	128 × 321	41.38311	1443.747
$10^{35/4}$	1	88.88239	128 × 321	48.77387	1821.661
10^9	1	102.3071	128 × 321	57.50461	2297.406
$10^{37/4}$	1	117.7822	128 × 449	67.82060	2896.298
$10^{38/4}$	1	135.6225	128 × 449	80.01178	3650.131

$10^{39/4}$	1	156.1963	128 × 449	94.42106	4598.740
10^{10}	1	179.9312	128 × 449	111.4542	5792.111
$10^{41/4}$	1	207.3119	128 × 449	131.5910	7293.324
$10^{42/4}$	1	238.9044	128 × 449	155.3995	9181.462
$10^{43/4}$	1	275.3612	128 × 449	183.5515	11555.93
10^{11}	1	317.4310	128 × 449	216.8420	14541.83
$10^{45/4}$	1	365.9813	128 × 641	256.2116	18296.30
$10^{46/4}$	1	422.0132	128 × 641	302.7737	23016.84
$10^{47/4}$	1	486.6804	128 × 641	357.8457	28951.78
10^{12}	1	561.6657	128 × 641	422.9866	36390.82
$10^{49/4}$	1	647.4534	128 × 641	500.0423	45793.62
$10^{50/4}$	1	746.8566	128 × 641	591.1965	57587.15
$10^{51/4}$	1	861.4431	128 × 769	699.0342	72424.84
10^{13}	1	994.2189	128 × 769	826.6155	91031.10
$10^{53/4}$	1	1147.050	128 × 769	977.5620	114458.7
$10^{54/4}$	1	1323.461	128 × 1025	1156.161	143907.6
$10^{55/4}$	1	1527.004	128 × 1025	1367.486	180935.2
10^{14}	1	1762.395	128 × 1025	1617.546	227422.7

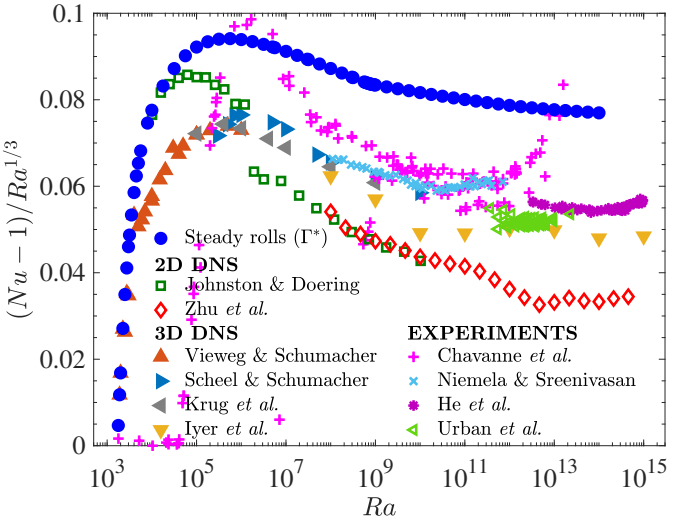

FIGURE 1S. Nu compensated by $Ra^{1/3}$ for steady rolls of Nu-maximizing aspect ratios Γ^* at $Pr = 1$, along with Nu from turbulent 2D and 3D DNS and experiments with estimated $Pr \in [0.6, 2]$. For horizontally periodic domains, 2D DNS with $(\Gamma, Pr) = (2, 1)$ were done by Johnston & Doering (2009) and Zhu *et al.* (2018), and 3D DNS with $\Gamma \geqslant 8$ and $Pr = 1$ were done by Vieweg & Schumacher (2020) and Krug *et al.* (2020). For DNS in cylinders of diameter-to-height ratio Γ_c, Iyer *et al.* (2020) used $(\Gamma_c, Pr) = (0.1, 1)$ and Scheel & Schumacher (2017) used $(\Gamma_c, Pr) = (1, 0.7)$. For laboratory experiments in cylinders, where the plotted data is truncated according to $Pr \in [0.5, 2]$, the domains and estimated Pr ranges are $\Gamma_c = 0.5$ and $Pr \in [0.6, 2]$ for Chavanne *et al.* (2001), $\Gamma_c = 4$ and $Pr \in [0.69, 1.84]$ for Niemela & Sreenivasan (2006), $\Gamma_c = 0.5$ and $Pr \in [0.79, 0.86]$ for He *et al.* (2012), and $\Gamma_c = 1$ and $Pr \in [0.95, 1.5]$ for Urban *et al.* (2014). Experiments used working fluids of low-temperature helium gas (Chavanne *et al.* 2001; Niemela & Sreenivasan 2006; Urban *et al.* 2014) or sulfur hexafluoride (He *et al.* 2012).

2. Comparison with turbulent convection

Figure 1S is nearly identical to figure 5 in the main text, comparing heat transport by Nu-maximizing steady rolls with transport by turbulent convection, except that more experimental data with Prandtl numbers further from 1 are included. In figure 1S the criterion for inclusion is an estimated Prandtl number of $Pr \in [0.5, 2]$ rather than the range $Pr \in [0.7, 1.3]$ in figure 5 of the main text. (In fact all of the estimated Pr are at least 0.6, so $Pr \in [0.6, 2]$ in figure 1S.) The working fluids in the experiments—gaseous helium or sulfur hexaflouride—are used near their critical points, leading to coupling and sensitive variation of material parameters that can be difficult to estimate. Faster variation of Pr with Ra is associated with increasing non-Oberbeck–Boussinesq effects as well; see Urban *et al.* (2011, 2012, 2014) for a discussion of experimental challenges. Data in figure 5 is truncated using the narrower range $Pr \in [0.7, 1.3]$ mainly to reduce non-Oberbeck–Boussinesq effects—we expect Pr alone to have a more modest effect, even over the wider range $[0.5, 2]$.

REFERENCES

Chavanne, X., Chilla, F., Chabaud, B., Castaing, B. & Hebral, B. 2001 Turbulent Rayleigh–Bénard convection in gaseous and liquid He. *Physics of Fluids* **13**, 1300–1320.

He, X., Funfschilling, D., Nobach, H., Bodenschatz, E. & Ahlers, G. 2012 Transition to the ultimate state of turbulent Rayleigh–Bénard convection. *Physical Review Letters* **108**, 024502.

Iyer, K.P., Scheel, J.D., Schumacher, J. & Sreenivasan, K.R. 2020 Classical 1/3 scaling of convection holds up to Ra = 10^{15}. *Proceedings of the National Academy of Sciences USA* **117**, 7594–7598.

Johnston, H. & Doering, C.R. 2009 Comparison of turbulent thermal convection between conditions of constant temperature and constant flux. *Physical Review Letters* **102**, 064501.

Krug, D., Lohse, D. & Stevens, R.J.A.M. 2020 Coherence of temperature and velocity superstructures in turbulent Rayleigh–Bénard flow. *J. Fluid Mech.* **887**.

Niemela, J.J. & Sreenivasan, K.R. 2006 Turbulent convection at high rayleigh numbers and aspect ratio 4. *Journal of Fluid Mechanics* **557**, 411–422.

Scheel, J.D. & Schumacher, J. 2017 Predicting transition ranges to fully turbulent viscous boundary layers in low Prandtl number convection flows. *Physical Review Fluids* **2**, 123501.

Urban, P., Hanzelka, P., Kralik, T., Musilova, V. & Srnka, A .and Skrbek, L. 2012 Effect of boundary layers asymmetry on heat transfer efficiency in turbulent Rayleigh-Bénard convection at very high Rayleigh numbers. *Physical Review Letters* **109**, 154301.

Urban, P., Hanzelka, P., Musilová, V., Králík, T., La Mantia, M., Srnka, A. & Skrbek, L. 2014 Heat transfer in cryogenic helium gas by turbulent Rayleigh–Bénard convection in a cylindrical cell of aspect ratio 1. *New Journal of Physics* **16**, 053042.

Urban, P., Musilová, V. & Skrbek, L. 2011 Efficiency of heat transfer in turbulent rayleigh-bénard convection. *Physical Review Letters* **107**, 014302.

Vieweg, P. & Schumacher, J. 2020 From 3D DNS with Pr = 1 and $\Gamma \geqslant 8$ by P. Vieweg and J. Schumacher. Private Communication.

Zhu, X., Mathai, V., Stevens, R.J.A.M., Verzicco, R. & Lohse, D. 2018 Transition to the ultimate regime in two-dimensional Rayleigh–Bénard convection. *Physical Review Letters* **120**, 144502.